Multiple Redox-Active Chlorophylls in the Secondary Electron-Transfer Pathways of Oxygen-Evolving Photosystem II[†]

Cara A. Tracewell[‡] and Gary W. Brudvig*

Department of Chemistry, Yale University, P.O. Box 208107, New Haven, Connecticut 06520-8107

Received August 3, 2008; Revised Manuscript Received September 14, 2008

ABSTRACT: Photosystem II (PS II) is unique among photosynthetic reaction centers in having secondary electron donors that compete with the primary electron donors for reduction of P_{680}^+. We have characterized the photooxidation and dark decay of the redox-active accessory chlorophylls (Chl) and β-carotenes (Car) in oxygen-evolving PS II core complexes by near-IR absorbance and EPR spectroscopies at cryogenic temperatures. In contrast to previous results for Mn-depleted PS II, multiple near-IR absorption bands are resolved in the light-minus-dark difference spectra of oxygen-evolving PS II core complexes including two fast-decaying bands at 793 and 814 nm and three slow-decaying bands at 810, 825, and 840 nm. We assign these bands to chlorophyll cation radicals (Chl^+). The fast-decaying bands observed after illumination at 20 K could be generated again by reilluminating the sample. Quantization by EPR gives a yield of 0.85 radicals per PS II, and the yield of oxidized cytochrome b_{559} by optical difference spectroscopy is 0.15 per PS II. Potential locations of Chl^+ and Car^+ species, and the pathways of secondary electron transfer based on the rates of their formation and decay, are discussed. This is the first evidence that Chls in the light-harvesting proteins CP43 and CP47 are oxidized by P_{680}^+ and may have a role in Chl fluorescence quenching. We also suggest that a possible role for negatively charged lipids (phosphatidyldiacylglycerol and sulfoquinovosyldiacylglycerol identified in the PS II structure) could be to decrease the redox potential of specific Chl and Car cofactors. These results provide new insight into the alternate electron-donation pathways to P_{680}^+.

In photosystem II, light energy is transferred from the antenna Chls in the Chl[1] -binding proteins CP43 and CP47 into the reaction center where the primary photochemical reactions are initiated. The primary electron donor Chl is most likely chlorophyll B_A (see Figure 1) (*1, 2*). The excited state of this chlorophyll drives charge separation, producing a reduced pheophytin ($Pheo_A^-$) and the chlorophyll cation radical species, P_{680}^+. The charge separation, P_{680}^+ $Pheo^-$, is stabilized by transfer of the electron to the protein-bound primary quinone, Q_A. Under normal conditions, P_{680}^+ is reduced by an electron from the oxygen-evolving complex (OEC), which consists of a redox-active tyrosine, Y_Z, and a tetranuclear Mn cluster (Mn_4), leading to the production of molecular oxygen from water oxidation (*3*). However, when electron donation from the OEC to P_{680}^+ is inhibited or

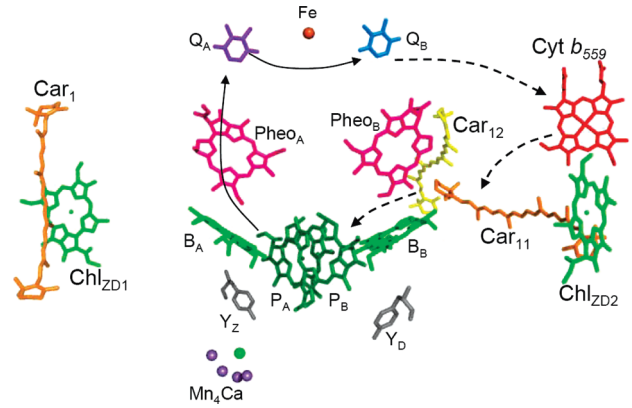

FIGURE 1: Model of electron-transfer reactions in photosystem II. The primary electron-transfer pathway is shown in solid arrows involving the photoactive primary electron-donor chlorophyll P_{680} (the cation is localized primarily on P_A), tyrosine Y_Z, and the tetramanganese cluster (Mn_4Ca). An alternate electron-transfer pathway, shown in dashed arrows, involves β-carotene (Car), the accessory Chl_{ZD2} in the D2 subunit, and cytochrome b_{559} (Cyt b_{559}). Car_{11} and Car_{12} are located in the D2 polypeptide, and Car_1 is located in the D1 polypeptide; of these, Car_{11}, is closer to Chl_{ZD2}, and Car_{12} is closer to the heme in Cyt b_{559} and, therefore, Car_{11} and/or Car_{12} are inferred to be electron-transfer intermediates. The phytyl tails of chlorophyll, pheophytin, and plastoquinone have been removed for clarity. This figure is adapted from the X-ray crystallographic structure described in ref (*14*) (PDB ID code 2AXT).

* To whom correspondence should be addressed. Phone: (203) 432-5202. Fax: (203) 432-6144. E-mail: gary.brudvig@yale.edu.

[†] This work was supported by the U.S. Department of Energy, Office of Basic Energy Sciences, Division of Chemical Sciences (DE-FG02-01ER15281), and an NIH predoctoral traineeship grant T32 GM008283 (C.A.T.). NSF Grant CHE-0215926 provided funds to purchase the ELEXSYS E500 EPR spectrometer.

[‡] Current address: Division of Chemistry & Chemical Engineering, California Institute of Technology, Pasadena, California 91125.

[1] Abbreviations: β-DM, β-dodecylmaltoside; Car, β-carotene; Car^+, β-carotene cation radical; $Car^\bullet$, β-carotene neutral radical; Chl, monomeric chlorophyll; Chl^+, chlorophyll cation radical; CP43, chlorophyll-binding protein encoded by psbC; CP47, chlorophyll-binding protein encoded by psbB; Cyt b_{559}, cytochrome b_{559}; D1, D1 polypeptide; D2, D2 polypeptide; DCBQ, 2,5-dichlorobenzoquinone; EDTA, (ethylenedinitrilo)tetraacetic acid; MES, 2-(*N*-morpholino)-ethanesulfonic acid; P_{680}, primary electron donor chlorophyll of PS II; PG, phosphatidyldiacylglycerol; PPBQ, phenyl-*p*-benzoquinone; PS II, photosystem II; SQDG, sulfoquinovosyldiacylglycerol; Y_D, redox-active tyrosine 160 of the D2 polypeptide; Y_Z, redox-active tyrosine 161 of the D1 polypeptide.

10.1021/bi801461d CCC: $40.75
Published on Web 10/14/2008

retarded, highly oxidizing P_{680}^+ ($E_m \sim 1.3$ V) can abstract an electron from other sources. The inventory of secondary donors includes Cyt b_{559}, tyrosine D (Y_D), β-carotene (Car), and redox-active chlorophylls called Chl_Z, identified as Chl_{ZD2} (and Chl_{ZD1} in spinach) (*4*).

The redox-active chlorophyll(s), carotenoids, and Cyt b_{559} comprise an alternate electron-transfer pathway that may protect PS II against uncontrolled oxidative reactions of the strong oxidant P_{680}^+ (*5*). Under physiological conditions, photooxidation of Cyt b_{559} and the redox-active tyrosine in the D2 polypeptide, Y_D, are observed. It has been found that Y_D is in redox equilibrium with the Mn cluster. The dark-stable state of the Mn cluster is the S_1 state, and the S_2 state can convert (relax) to the S_1 state by oxidizing Y_D to form the dark-stable radical $Y_D^\bullet$ (*6*). At low temperature, it was found that the rate of electron donation to P_{680}^+ from Y_D is pH dependent (*7*). The electron-transfer reaction is coupled to proton transfer, which is slow at low temperatures due to an activation barrier, whereas the rate is increased at high pH presumably because the tyrosine is already deprotonated. Interconversion between the oxidized states of Y_D and Car is not observed at low temperature, implying that Car^+ is not in redox equilibrium with $Y_D^\bullet$. Therefore, Y_D is not part of the secondary electron-transfer pathway involving Car, Chl, and Cyt b_{559} but a competing secondary electron-donation pathway.

On the basis of spectroscopic evidence from Mn-depleted PS II samples, it has been reported that one to two Chl (*8, 9*) and two Car molecules are secondary electron donors (*10, 11*). These molecules were predicted to be located between the special pair Chls (P_A and P_B) and the heme of Cyt b_{559}, which is the preferential secondary electron donor to P_{680}^+ (*12, 13*). Previous studies on Mn-depleted PS II samples by our laboratory indicated that one oxidized Chl was located in the D1 polypeptide ligated to His118 (*9*). We interpreted a second peak in the Chl^+ spectrum of Mn-depleted spinach PS II membranes to be a second Chl^+, possibly ligated to the D2-His117 (*8*). Because these Chls are >30 Å from the special pair Chls, an intermediate molecule must participate in the electron-transfer reactions. This was hypothesized to be a Car molecule (*12*). The most recent, and highest resolution, crystal structure of PS II by Loll et al. reveals one all-trans Car molecule in the D1 polypeptide near Chl_{ZD1} and two all-trans Car located in the D2 polypeptide region near Chl_{ZD2} and the heme of Cyt b_{559}; the latter two Car bridge the distance from Cyt b_{559} to the special pair Chls (*14*). The structure of PS II agrees with the proposal that Car is an intermediate in the photooxidation of Cyt b_{559}. Kitajima and Noguchi found that Chl^+ formation can still occur even when Car is photobleached in PS II (*15*). This result suggests that the bleached Car molecules are not located in the D2 polypeptide.

The Car molecules located in the D2 polypeptide are in close proximity to the Car molecules in CP43, suggesting the possibility of oxidation of Chls in the antennae via hole hopping (*14*). One D2 carotenoid, Car_{11}, is located 6.8 Å from Chl_{ZD2} (labeled Chl_7 in the X-ray crystal structure) and is closest to the heme of Cyt b_{559} (11.7 Å). The second D2 carotenoid, Car_{12}, is 12 Å from Car_{11} and only 4.9 Å from Car_{13}, which is located in the antennae protein CP43. Vasil'ev et al. first proposed that Chl_{ZD1} could be oxidized via the Car in D2 through several Chls in CP43 (*16*). Calculations of energy transfer between the Chls in PS II revealed that a cation radical located on the Chl molecules in CP43 and CP47 could have considerable impact on the energy-transfer dynamics of PS II (*17*). However, spectroscopic evidence for such a pathway has been lacking.

Several studies have measured the distance between Chl^+ and other locations in PS II, such as the nonheme iron or tyrosine D, using magnetic resonance techniques. For example, Koulougliotis et al. determined the distance between the nonheme iron and Chl_Z^+ to be 39.5 ± 2.5 Å using saturation-recovery EPR (*18*). PELDOR measurements predicted a distance between Q_A and Chl^+ to be 34 Å (*19*). Electron spin echo measurements determined the distance between $Y_D^\bullet$ and Chl^+ (generated at 200 K) to be 29.4 ± 0.5 Å (*20*) and, using high-field W-band EPR and deuterium labeled PS II samples, the Chl^+ and Car^+ spectra could be resolved; the distance between Chl_Z^+ and the nonheme iron in Mn-depleted *Synechocystis* PS II was determined to be >40 Å (*21*). Most of this work was done on Mn-depleted PS II, and the temperature of illumination varied between 20 and 200 K. However, as the near-IR spectra presented herein indicate, the composition of the Chl^+ species and Car^+ species formed in the sample is temperature dependent and, due to differences in stability, time dependent as well (*8, 12*). Therefore, it is likely that the distances determined by these methods reflect a mixture of Chl^+ and Car^+ radicals present in the sample.

The angular dependence of Chl^+ in spinach PS II membranes was measured at 198 K and found to be perpendicular to the membrane plane (*22*). This result excludes the two core Chls, B_A and B_B, but nearly all of the Chl in CP43 and CP47 and the accessory Chls (Chl_{ZD1} and Chl_{ZD2}) are oriented perpendicular to the membrane plane (*14*).

The electrostatic environment of the Car molecules and the Chl molecules located in the D1 and D2 polypeptides in the Loll et al. PS II structure was used to calculate the E_m values (*23*). The calculated E_m values for Chl_{ZD1} and Car_1 are higher than for Chl_{ZD2} and Car_{11} or Car_{12}, suggesting that an oxidizing equivalent would be preferentially localized on the D2 side of PS II.

In this manuscript, we describe near-IR light-minus-dark difference spectra of O_2-evolving *Synechocystis* PS II core complex samples (not treated with hydroxylamine to reduce the Mn_4Ca cluster). These samples exhibit the formation of multiple near-IR absorption peaks. We attribute these spectroscopic features to distinct photooxidized chlorophyll cation radicals having different kinetic properties. We show that the Chl^+ are intermediates of the secondary electron-transfer pathway in which Cyt b_{559} is the electron donor. We also present a model for Chl^+ formation in the antennae proteins CP43 and CP47.

MATERIALS AND METHODS

Chemicals and Reagents. 2-(*N*-morpholino)-ethanesulfonic acid (MES) and β-dodecyl maltoside (β-DM) were purchased from U.S. Biochemicals. Piperazine-*N*,*N*′-bis(4-butanesulphonic acid (PIPBS) was purchased from GFS Chemicals Inc. Phenyl-*p*-benzoquinone (PPBQ) was purchased from Aldrich and recrystallized twice in ethanol. Stock solutions of PPBQ and potassium ferricyanide (25 mM each) were

prepared in DMSO and water, respectively, and frozen until use. Ascorbate was purchased from Aldrich.

Protein Preparation. His-tagged PS II core particles were isolated from *Synechocystis* PCC 6803 cells as described (*24*). The final buffer contained 20% glycerol, 15 mM NaCl, 50 mM MES, pH = 6.0, unless otherwise indicated.

Oxygen-Evolving Assays. O_2-evolving activity of purified PS II core complexes was assayed using a Clark-type oxygen electron in the presence of 250 μM DCBQ and 1 mM potassium ferricyanide in a buffer containing 0.4 M sucrose, 20 mM $CaCl_2$, 5 mM $MgCl_2$, and 0.03% β-DM and was typically between 2000 and 2900 μmoles O_2 (mg Chl)$^{-1}$ hr^{-1}. The O_2-evolving activity was reduced to about 40% of the original activity in buffer containing 60% glycerol, and the O_2-evolving activity is reduced to ~10% at pH 8.5, but in both cases, the activity is restored when the sample is returned to the original buffer at pH = 6.0.

Sample Treatments. Mn-depleted PS II samples were prepared by washing into a buffer containing 50 mM MES (pH = 6.0), 15 mM NaCl, 1 mM $CaCl_2$, and 0.4 M sucrose, and 0.03% β-DM (buffer A). The sample was diluted 1:1 with buffer A, which also contained 10 mM hydroxylamine and 10 mM Na_2EDTA, and incubated in the dark for 30 min stirring on ice to allow for the reduction of the tetramanganese cluster by hydroxylamine. Free manganese was removed by washing with buffer A containing 5 mM Na_2EDTA. Mn-depleted PS II core complexes were also prepared by incubating for 4−12 h on ice with buffer A containing 100 mM ascorbate instead of hydroxylamine. Free manganese was removed by the wash steps described above.

For low-temperature measurements, PS II samples were transferred to a buffer containing 20 mM $CaCl_2$, 5 mM $MgCl_2$, 63% (v/v) glycerol, and 50 mM MES at pH 6.0 (buffer B) unless otherwise indicated. Prior to freezing, PS II samples were treated with 5 mM ferricyanide to oxidize Cyt b_{559}.

Tyrosine D was photooxidized to form $Y_D^{\bullet}$ by the following procedure: PPBQ was added to PS II samples to a final concentration of 500 μM, then samples were incubated in darkness on ice for 30 min, illuminated at room temperature for 30 s to photooxidize Y_D, incubated on ice in the dark for 3 min to allow for any unstable charge separations resulting from Y_Z oxidation to decay, and then frozen.

UV−Visible−Near-IR Optical Spectroscopy. A Perkin-Elmer Lambda 20 spectrometer was used to make optical spectroscopic measurements in the UV−visible and near-IR. Low-temperature optical measurements were made with an Oxford Instruments Optistat liquid helium cryostat. Polyethylene cuvettes with a 1.0 cm path length and 0.4 cm width (Fisher Scientific) were used for low-temperature optical measurements. PS II samples were mixed to homogeneity with buffer B in the cuvette using a home-built Teflon plunger machined to fit in the cuvette. A 150 W quartz-halogen lamp filtered by a 6 in water bath and a heat-absorbing filter (Schott KG-5) was used to illuminate samples. A Schott-Fostec randomized fiber optic bundle was used to direct the light into the cryostat. For specified experiments, a Uniblitz electronic shutter was placed between the filters and the fiber optic bundle and operated by a shutter controller to produce short flashes of white light between 0.1 ms and 100 s in length.

The PS II samples were dark adapted for 1 h on ice and then slowly frozen in the dark by setting the cuvette inside a brass cylinder in contact with a liquid nitrogen bath. A sample was cooled slowly over a period of 15 min in the dark to form an optically clear glass. The sample was then rapidly transferred to the cryostat with minimal light exposure. Illumination experiments were performed on samples that were equilibrated at the specified temperature for at least 60 min or until baseline changes were no longer observed in the spectra of the nonilluminated sample. All spectra collected after illumination are referenced to the dark spectrum measured at the same temperature to avoid contributions from spectral changes in the background due to temperature effects.

The yield of reduced Q_A was determined using the C550 signal, an electrochromic shift of a Pheo band due to the charge of an electron on Q_A (*25*), which serves as a reporter of Q_A^-. The C550 signal was quantified by measuring the peak-to-peak difference of the derivative-shaped feature and converted to concentration using the extinction coefficient 3.4 mM^{-1} cm^{-1} (*26*). The quantity of photooxidized Cyt b_{559} was calculated using the extinction coefficient 17.5 mM^{-1} cm^{-1} (*27, 28*).

Spectral Simulations. The program Microcal Origins 6.0 was used to simulate the near-IR absorption data, to analyze the decay kinetics and to plot all spectra. No filtering or smoothing of spectra was used, but, for UV−visible absorbance (light-minus-dark) spectra, three scans were averaged for each spectrum shown. Difference spectra were obtained only by subtraction of spectra taken at the same temperature from the same sample.

EPR Spectroscopy. X-band EPR measurements were conducted on a Bruker ELEXSYS E500 EPR spectrometer equipped with an Oxford ESR 900 He-flow cryostat and a Super High Q (SHQ) cavity. Samples were illuminated as described for optical experiments, and all spectra were collected in the dark. Radical yields per PS II were determined by double integration of the derivative EPR signals and calibrated to photooxidized tyrosine D ($Y_D^{\bullet}$).

Electron-Transfer Rates. We analyzed the near-IR absorption spectra of O_2-evolving PS II with respect to the locations of the chlorophylls and carotenoids modeled in the X-ray crystal structure (*14*). Because of the long distances involved, it was assumed that the electron transfer is nonadiabatic. The rates will depend strongly on the distance because the coupling is limited by the small electronic overlap between the donor and acceptor. Rates of long-distance electron transfer in proteins has been approximated well by the empirical equation developed by Dutton and co-workers (*43*) based on Marcus theory:

$$\mathrm{Log}_{10}\, k_{et} = 13 - 0.6(R-3.6) - 3.1(\Delta G + \lambda)^2/\lambda \quad (1)$$

where R is the edge-to-edge distance between donor and acceptor, ΔG is the free energy difference between donor and acceptor, and λ is the reorganization energy. We measured the distances between the Chls and Cars in the Loll et al. (*14*) X-ray crystal structure of PS II (3.0 Å resolution). The calculated potentials of Ishikita and Knapp (*29*) of PS II Cars and Chls and the measured potential of Q_A^- were used to estimate ΔG. The reorganization energy was estimated to be between 0.5 and 0.7 eV, values that have been used in other reaction center electron-transfer reactions. We expect the reorganization energy to be a low

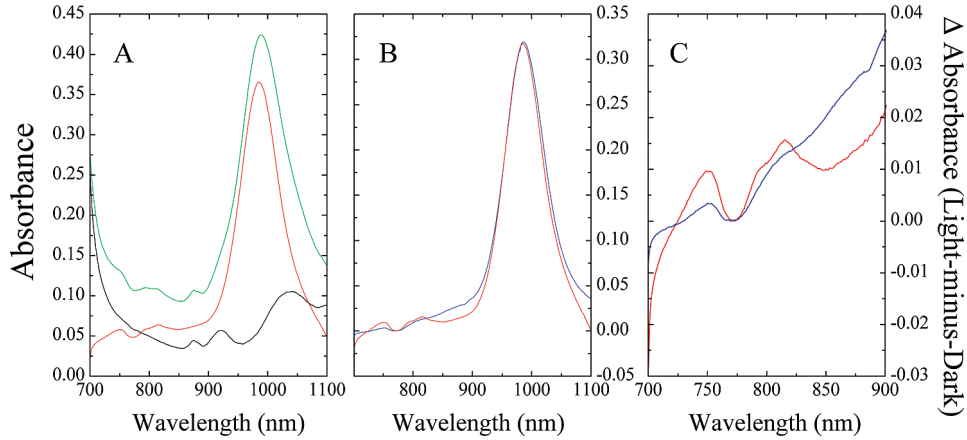

FIGURE 2: Near-IR spectrum of O_2-evolving *Synechocystis* PS II prior to illumination (black) after illumination (green) and the difference spectrum showing light-induced species formed by illumination at 20 K (red) (A). Light-minus-dark difference spectra of Mn-depleted *Synechocystis* PS II (blue) and O_2-evolving *Synechocystis* PS II (red) are shown in (B). Both samples were treated with 5 mM ferricyanide prior to freezing and illuminated for 15 min at 20 K. Spectra are scaled to the same Chl concentration (2.82 mg Chl/mL), and the cuvette path length is 1.25 mm. The 700−900 nm region of (B) is expanded in (C).

value considering that the cofactors are buried within the hydrophobic core of the membrane protein.

To clarify, the notation used here to identify CP43 and CP47 Chls from the X-ray crystal structure is based on the numbering in the PDB file where the last two numbers of the molecule code are used as a subscript (*14*). For example, the Chl molecule in CP43 identified as Cla22 in the structure coordinates is abbreviated here as Chl_{22}. Also, in the case of the Chls bound to His118 in the D1 polypeptide and His117 in the D2 polypeptide, the abbreviations of Chl_{ZD1} and Chl_{ZD2}, respectively, are used.

RESULTS

Identification of Multiple Near-IR Absorbing Species in O_2-Evolving Photosystem II. O_2-evolving *Synechocystis* PS II core complexes were illuminated for 15 min at 20 K, resulting in the formation of a charge-separated state composed of a mixture of oxidized species (Car^+ and Chl^+) and reduced species (Q_A^-). The near-IR absorbance spectra of O_2-evolving PS II are shown in Figure 2. A difference spectrum of O_2-evolving PS II before illumination, also called the dark spectrum (shown in black), and after illumination, also called the light spectrum (shown in green), reveals the light-generated species (see Figure 2A). The nonilluminated spectrum has broad features at 1030, 920, and 875 nm that arise from the O−H stretching overtones of water. The low-energy Q_Y absorption band of the neutral Chls in the protein contributes to the rising baseline near 700 nm. The light-minus-dark difference spectrum (red) of the O_2-evolving PS II core complexes is compared to the light-minus-dark difference spectrum of Mn-depleted PS II core complexes (blue) in Figure 2B,C. The spectra are scaled to the same concentration of PS II based on 38 Chls per PS II (*30*). The carotenoid cation radical spectra are similar in the two samples with the exception of the Car^+ vibronic band at ~880 nm and also the low-energy tail near 1100 nm. The increase in absorbance of the Car^+ peak at the low-energy and high-energy portions of the spectrum of Mn-depleted PS II compared to that of O_2-evolving PS II may be due to increased heterogeneity in the structure of the Mn-depleted sample, which is reflected by increased heterogeneity of the carotenoid cation radicals. The two spectra are noticeably different in the region of the chlorophyll cation radicals, expanded in Figure 2C, where a stronger absorbance at 814 nm and a shoulder at 793 nm appear in the near-IR difference spectrum of O_2-evolving PS II core complexes. There is also an increase in the intensity of the 750 nm absorbance peak, attributed to Car neutral radicals (*31*). We studied the formation and decay of the light-induced near-IR spectral features of O_2-evolving PS II core complexes and the results are described below.

We monitored the stability over several hours in the dark at 20 K of the light-generated species. The initial light-minus-dark spectrum (black) for O_2-evolving PS II is shown in Figure 3A,B (also shown in Figure 2) in comparison to the light-minus-dark spectrum recorded 30 min later (red) and 8 h later (green). The difference spectrum of the initial spectrum and 30 min later (Figure 3C, black) shows that 750, 793, and 814 nm peaks decay substantially 30 min after illumination. A difference spectrum of the spectrum recorded 30 min later and the spectrum measured after 8 h (Figure 3C, red) shows that, during an additional 7.5 h, the 793 nm peak and the 750 nm peak continue to decay. Also during this time, the Car^+ peak decays as observed previously for Mn-depleted PS II and the bleach near 700 nm due to neutral Chls recovers. Two broad near-IR absorption features at ~810 and ~825 nm remain after several hours incubation in the dark, and a portion of the 750 nm peak that decays more slowly also remains. The spectra we present here for O_2-evolving PS II core complexes from *Synechocystis* PCC 6803 are different from hydroxylamine-treated Mn-depleted PS II samples in the following ways: in Mn-depleted PS II samples, a broad Chl^+ peak centered at 814 nm formed upon illumination and remained for several hours at 20 K, whereas, in O_2-evolving PS II core complexes, the Chl^+ peak at ~800 nm was sharper, exhibited two maxima, and exhibited rapidly decaying Chl^+ species that were not observed in Mn-depleted PS II samples (*8*).

The near-IR absorption spectra in Figure 3 indicate that the light-induced near-IR absorptions observed in O_2-evolving PS II arise from several kinetic components. The difference spectra and kinetic plots in Figure 4 illustrate that there are three rapidly decaying bands (λ_{max} = 750, 793, and 814 nm) and two distinct fast kinetic components. A broad

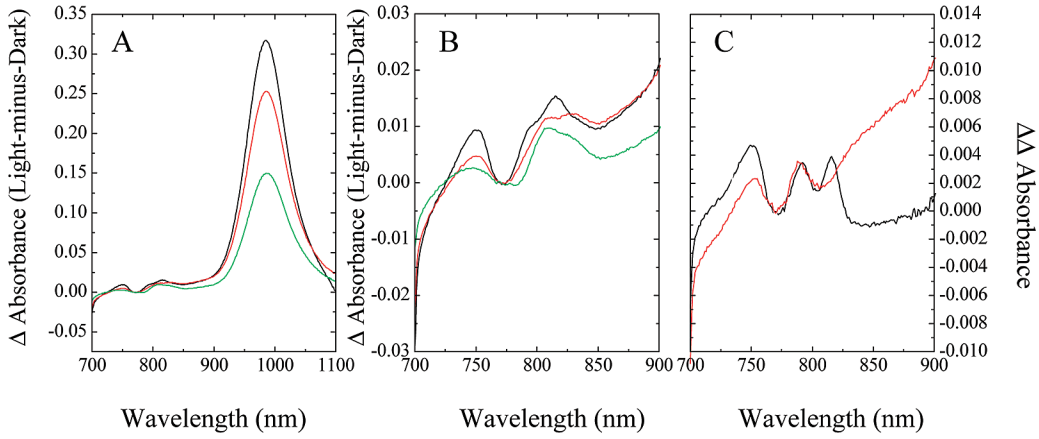

FIGURE 3: Near-IR light-minus-dark difference spectrum of O_2-evolving *Synechocystis* PS II illuminated by white light for 15 min at 20 K (A) and the same spectra in the 700−900 nm range (B). In both panels, the initial spectrum (black), the spectrum recorded 30 min later (red), and the spectrum recorded 8 h later (blue) are shown. The difference spectra between the initial spectrum and the spectrum recorded 30 min later (black) and between the spectra recorded 30 min and 8 h later (red) are shown in (C). Chl concentration is 2.82 mg/mL, and sample path length is 1.25 mm.

absorption feature at ~840 nm is also observed, which grows in as these fast components decay and then subsequently decays at a slow rate. This analysis indicates that multiple Chl^+ species are formed in the PS II sample and that these species have significantly different stabilities. Thus, the near-IR spectra of O_2-evolving PS II core complexes are composed of multiple overlapping peaks in the Chl^+ absorption region of the spectrum.

We have used the variable decay kinetics of the Chl^+ species to deconvolute the overlapping spectral components. At 20 K, most of the spectral changes occur within the first 30 min after illumination. After several hours, the near-IR light-minus-dark difference spectrum does not change appreciably. To examine the time-dependent absorption changes occurring within the first few hours more carefully, the light-minus-dark difference spectrum collected 5.5 h after illumination was subtracted from the earlier light-minus-dark spectra to generate a series of double difference spectra (shown in Figure 4A,B). The absorption changes in the double difference spectra are plotted as a function of time in Figure 4C for the wavelengths 840, 814, 793, 750, and 701 nm (indicated by arrows in Figure 4A,B). The double difference spectra are divided into two sections shown in parts A and B of Figure 4, respectively, at the time indicated by the dashed line in Figure 4C, after which there is no additional formation of the 840 nm species. The double difference spectra plotted for the period just after illumination up to ~1800 s (Figure 4A) has isosbestic points at 715, 770, 825, and 890 nm. As the spectra and single-wavelength plots indicate, the fast-decaying species at 750, 793, and 814 nm decay at different rates. The 814 nm species decays the most rapidly having a half-time of 220 s (Figure 4E), and it has completely decayed within 30 min after the lamp is shut off. The 793 nm species (Figure 4F) and the 750 nm species (Figure 4D) decay less rapidly ($t_{1/2}$ = 570 s and $t_{1/2}$ = 700 s, respectively). During the rapid decay phase, another species at ~840 nm is formed, reaching a maximal value after 30 min. The 840 nm rise can be fit to two formation components ($t_{1/2}$ = 200 s and $t_{1/2}$ = 700 s) and a decay component ($t_{1/2}$ = 7000 s). The data suggest that each of these peaks arises from a separate species because they decay at different rates. The double difference spectra for the time period of 30 min after illumination to 5.5 h after illumination has isosbestic points at 730 and 770 nm (Figure 4B), indicating that the interconversion of components (or lack thereof) is different at longer times than in the first 30 min.

It is apparent that there are at least two possible mechanisms for the decreasing Chl^+ absorption features: Chl^+ decay could occur either by oxidation of another Chl or Car or by charge recombination with Q_A^-. Both of these processes depend on distance, either the distance between the oxidized Chl species and other nearby Chl or Car molecules (hole migration) or the distance of Chl^+ to Q_A^- (charge recombination). The rise and decay of absorption at 840 nm is clear evidence for hole migration. After the 814 nm peak has decayed completely, there is no additional formation of the 840 nm species, suggesting that the 814 nm Chl^+ converts into the 840 nm Chl^+.

Figure 5 shows a Gaussian deconvolution of the spectrum of rapidly decaying Chl^+ species shown in Figure 3C and the spectrum of the more stable Chl species shown in Figure 3B. Three Gaussians were fit to the fast-decaying Chl^+ spectrum, and the peak maxima are 750, 793, and 814 nm (Figure 5B). Five Gaussians were used to fit the slow-decaying Chl^+ spectrum, and the peak maxima are 742/754, 810, 825, and 840 nm. The peak positions and widths obtained from these fits were used (and not allowed to vary in the fit) to deconvolute spectra in the following sections. Using five Gaussian curves for the Chl^+ bands (793, 810, 814, 825, and 840 nm), one Gaussian for the neutral Chl Q_Y band bleach, two Gaussians for the Car neutral radical bands (742 and 754 nm), two Gaussians for the Car^+ absorbance peaks (Car_A^+, 984 nm and Car_B^+ at 1029 nm (*11*)), and an additional Gaussian for the Car^+ vibronic band at 890 nm, for a total of 11 Gaussian curves, the spectra described below were simultaneously fit using the program Microcal Origin 6.0. Linear constraints were also included such that the Gaussian deconvolution composition of a fit of the difference spectrum was the difference of the Gaussian deconvolution of the two spectra from which it was derived. From the deconvoluted spectra, we calculated the chlorophyll cation radical yield in PS II using the extinction coefficient 7000 M^{-1} cm^{-1} at the near-IR wavelength of maximum absorbance for each Gaussian (*32*). We calculated the yield of Car^+ using the extinction coefficient 160000 M^{-1} cm^{-1} at the near-IR wavelength of maximum absorbance for each Gaussian (*33*).

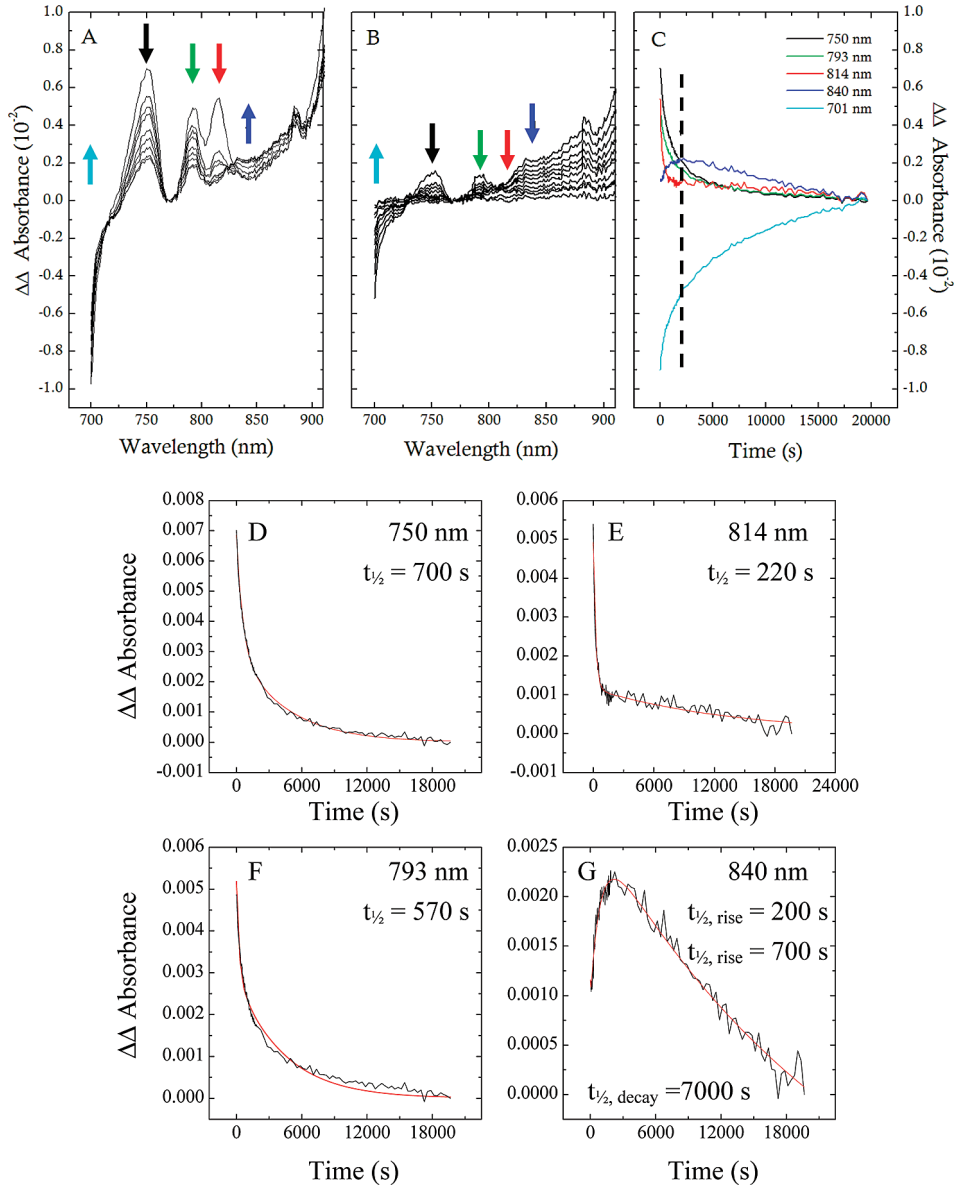

FIGURE 4: Near-IR double difference absorbance spectra of O_2-evolving *Synechocystis* PS II, referenced to spectra recorded 5.5 h after illumination. The absorbance change at wavelengths 701 nm (cyan), 750 nm (black), 793 nm (green), 814 nm (red), and 840 nm (blue), indicated by arrows in (A) and (B), are plotted as a function of time after the illumination in panel (C). The dashed line in panel (C) indicates the time division at which spectra are plotted in panels (A) and (B) for short and long times, respectively. Exponential decay fits to single-wavelength data shown in (C) for 750 nm (D), 814 nm (E), 793 nm (F), and 840 nm (G).

Because of the instability of cation radicals in solution, there is some uncertainty associated with these values, but they appear to be good approximations to the values of these species in PS II based on agreement within about 20% of the values estimated from the optical spectra and the yield of radicals determined by EPR spectroscopy (see below).

Formation of Chl$^+$, Car$^+$- Short Illumination Times. The decay of the near-IR absorption bands between 700−900 nm in PS II is complex. To further disentangle the spectra of these species, we measured the formation of the near-IR absorption signals and the C550 feature that indicates the quantity of Q_A^- formed (see Materials and Methods) in O_2-evolving PS II core complexes. The near-IR light-minus-dark difference spectra are shown in Figure 6A,B. After brief illumination of the sample (0.5 ms to 100 s), the Car$^+$ absorbance peak at 983 nm and the 814 and 750 nm peaks form with a shoulder at 793 nm. By using the Gaussian curves described above for the Chl$^+$ and Car neutral radical peaks, we simultaneously fit the series of spectra with the following constraints: the peak positions and widths were the same for all spectra. Peak positions and peak widths were obtained from the fast-decaying and slow-decaying spectra. An example of a deconvoluted spectrum (measured after 10 s illumination) is shown in Figure 6C,D. The absorbance maximum of each Gaussian curve was used to calculate the cation radical yield per PS II using the extinction coefficients given above (Figure 6E,F). On the basis of the spectral deconvolutions, the order of Chl$^+$ and Car neutral radical formation in the O_2-evolving samples is, first, the 814, 793, and 750 nm peaks and then subsequently the 825, 810, and 840 nm peaks are formed (see below). Simulations of the spectra indicate that the 810, 825, and 840 nm absorption bands do not begin to contribute significantly until after ~100 s of illumination. In this set of experiments, the absorbance maximum of the Car$^+$ peak is 983 nm, which is similar to the absorbance maximum after longer periods of illumination.

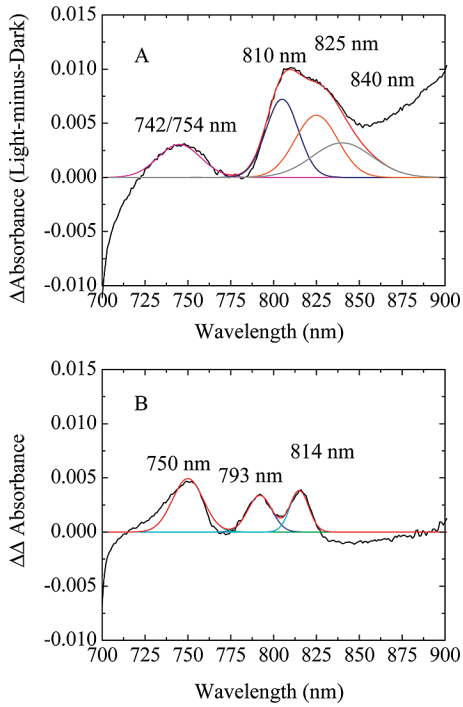

FIGURE 5: (A) Gaussian deconvolution of the slow-decaying species identified in Figure 3B. (B) Gaussian deconvolution of the fast-decaying species identified in Figure 3C.

Because the absorbance maximum and width of the carotenoid cation radical peak remain the same after each illumination, the composition of the peak is assumed to be the same ratio of the two redox-active Car molecules identified previously (*11*) for illuminations up to 100 s.

Formation of Chl$^+$, Car$^+$- Long Illumination Times. As shown above, the near-IR light-minus-dark difference spectrum depends on the length of time the sample is illuminated. The striking difference between near-IR spectra measured after short illuminations, shown in Figure 6B, and the spectrum measured after 15 min illumination, shown in Figure 3B, is the intensity of the absorption feature near 840 nm. Although the Car$^+$ vibronic band also contributes to this region, the experiments shown in Figures 3 and 4G indicate that the 840 nm feature is formed through the interconversion of cation radicals.

If the fast-decaying species are intermediates in the formation of the long-wavelength Chl$^+$ species, then the amount of the fast-decaying species observed in the difference spectrum should decrease with additional illumination. We measured spectra after several cycles of illumination and dark incubation and the results are shown in Figure 7. First, the PS II sample was illuminated for 1 min and then spectra were collected approximately every 30 s in the dark for 30 min. After this dark incubation period, the PS II sample was subsequently reilluminated for an additional 5 min and spectra were collected for 30 min in the dark. This procedure was repeated on the same sample at 20 K for 10 and 15 min illuminations. The initial light-minus-dark difference spectrum for the each illumination is shown in Figure 7. After additional illumination of the O_2-evolving PS II sample, absorption features at 810 and 825 nm increase. The absorption at ~850 nm, due to Car$^+$ and Chl$^+$ features, decreases in the near-IR absorption spectrum. Although the Car$^+$ absorbance peak is near the maximal value after 100 s of illumination, the light-minus-dark spectrum measured is not identical to the spectrum recorded after 15 min of illumination. The peak maximum remains at 983 nm throughout the illumination series. But, with additional illumination, the width of the Car$^+$ absorption peak increases (Figure 7 inset). The increase in Car$^+$ peak width is due to the additional formation of an absorbance feature at 1010 nm (and possibly bleaching of the Car$^+$ 983 nm band, which suggests conversion of Car$^+$ from a short- to a long-wavelength Car$^+$ form is occurring (*11*)). By comparing the species that form and decay after a series of illuminations of increasing length, we observed that the 793 and 814 nm species can convert into longer-wavelength species. But it is not a total conversion, and additional illumination does not drive all of the fast-decaying species to the slow-decaying species.

EPR Spectroscopy. The X-band EPR spectrum of O_2-evolving PS II core complexes was measured as a function of the illumination time at 30 K, and the results are shown in Figure 8. At very short illumination times, the *g*-factor of the low-intensity spectrum was similar to oxidized tyrosine D (see Figure 8A). (For EPR spectra, see Supporting Information Figure S1.) Rapid oxidation of tyrosine D has been measured at high pH (*34*). It has been hypothesized that electron transfer can occur if the tyrosine is already deprotonated. At X-band EPR, the *g*-tensors of Car$^+$ and Chl$^+$ in PS II are unresolved and the derivative-shaped spectra are nearly indistinguishable; however, the line widths are 9.5 and 10.4 G for Car$^+$ and Chl$^+$, respectively, measured in spinach PS II membranes (*12*). The line width of the EPR spectrum measured after 15 min is 10.2 G (Figure 8B), which is between these two values, as expected for a mixture of Car$^+$ and Chl$^+$. By comparing the EPR line shapes of the spectrum obtained after 50 ms illumination to the spectrum obtained after 1000 s illumination, it can be seen that a portion of the 50 ms spectrum is composed of oxidized tyrosine D. As the intensity of the EPR signal increases with additional illumination of the sample at 30 K, the *g*-factor shifts to a value similar to those reported for Car$^+$ and Chl$^+$ (Figure 8A). After 1000 s, the light-induced EPR signal has reached a steady-state value of 0.85 radicals per PS II (Figure 8C). If it is assumed that oxidized Y_D formed during early illumination times at 30 K is still present in the sample after the signal intensity has reached a steady-state value, then the $Y_D^{\bullet}$ signal contributes less than 1% of the total radical yield per PS II. The decay of the EPR spectrum was monitored in the dark (see Figure 8D) and can be fit to a biexponential decay curve with half-lives of 675 and 5200 s.

Formation of Q_A^- and Photooxidized Cytochrome b_{559}. Each charge-separated state formed by illumination at low temperature is composed of an electron acceptor that has been determined to be Q_A in PS II. The redox state of Q_A was monitored through the electrochromic shift of the pheophytin absorption band at 540 nm The difference spectrum has a derivative line shape and is called the C550 signal and is a linear indicator of Q_A reduction (*25*). We measured the accumulation of Q_A^- by monitoring the appearance of the C550 signal in O_2-evolving PS II core complexes as a function of illumination time, and the spectra are shown in Figure 9A. The yield of Q_A^- reaches a maximal value of 1 per PS II reaction center after 100 s of illumination (Figure 9B). As described above, the yield of certain Chl$^+$

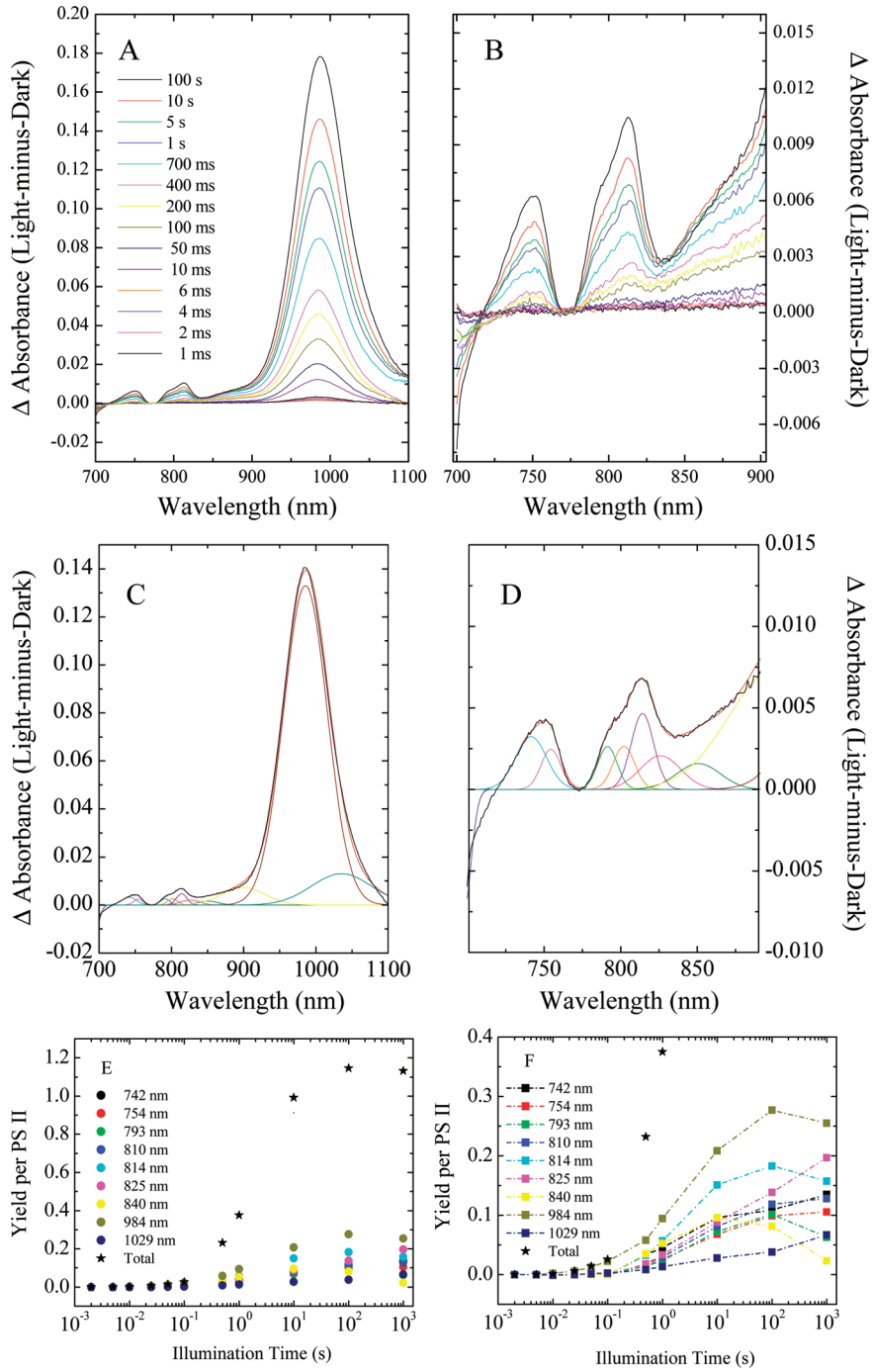

FIGURE 6: (A) Near-IR light-minus-dark difference spectra of O_2-evolving *Synechocystis* PS II measured after short illuminations at 20 K by white light from a 150 W lamp. Sample was illuminated for: 1 ms, 2 ms, 4 ms, 6 ms, 10 ms, 50 ms, 100 ms, 200 ms, 400 ms, 700 ms, 1 s, 5 s, 10 s, and 100 s. (B) 700−900 nm region is expanded. Chl concentration is 0.15 mg/mL. Example of a Gaussian deconvoluted spectrum (measured after 10 s illumination) is shown in (C) and (D). Eleven Gaussians were used to simulate the spectra: Chl^+ peak positions were: 742, 754, 793, 810, 814, 825, and 840 nm. Car^+ peak positions were: 984 nm, 1029 nm, and Car^+ vibronic band at 890 nm. Radical yield of each near-IR species per PS II (E). Radical yields were calculated with the extinction coefficients given in the text. Expanded in (F) to show Chl^+ yields.

species continues to increase upon further illumination of the PS II sample while the yield of other Chl^+ and Car^+ species decreases. Because of uncertainty in the values of the extinction coefficients of Car^+ and Chl^+, it was not clear whether additional charge-separated states continue to form after long illumination or whether the changes in the near-IR spectra are due to conversion of one cation radical species into another. The measurement of Q_A^- clarifies that the maximum number of charge separations is formed within 100 s and, therefore, any spectroscopic changes that occur after this are due to conversion between charge-separated states.

Photooxidation of Cyt b_{559} also occurred during illumination at 20 K, although the sample was treated with 5 mM ferricyanide prior to freezing (Figure 9A). It is not surprising that a portion of Cyt b_{559} was not oxidized by 5 mM ferricyanide because high-, intermediate-, and low-potential forms of Cyt b_{559} have been documented in PS II samples.

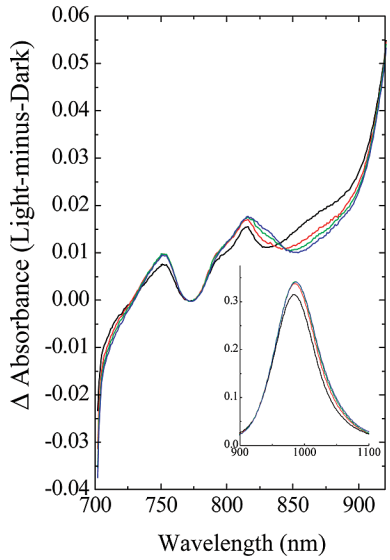

FIGURE 7: Near-IR light-minus-dark difference spectra of O_2-evolving *Synechocystis* PS II following a series of long illuminations at 20 K. The spectra were recorded following illumination for 1 min (black), 5 min (red), 10 min (green), and 15 min (blue).

A certain fraction of high-potential Cyt b_{559} may not be oxidized by the exogenous oxidant. Here, the maximal value of photooxidized Cyt b_{559} formed by low-temperature illumination at 20 K is 15% (Figure 9B).

DISCUSSION

PS II generates a strong oxidant, P_{680}^+, which is capable of oxidizing Chl and Car molecules. Previously, the alternate electron-transfer pathway intermediates were studied in Mn-depleted PS II samples because this state was thought to mimic centers with impaired O_2-evolution (*8, 12*). However, we have found that the light-induced near-IR spectrum of O_2-evolving *Synechocystis* PS II core complexes has additional features in the 700−900 nm region, where chlorophyll and carotenoid radicals absorb, and that some of these species exhibit much faster formation and decay kinetics than in Mn-depleted PS II. We attribute the near-IR signals formed in O_2-evolving PS II to Car^+, Chl^+, and $Car^\bullet$ species that absorb near 980, 820, and 750 nm, respectively. Both Car and Chl cation radicals have been previously studied in Mn-depleted PS II (*4*). The 750 nm absorbance feature observed here was also observed in Mn-depleted PS II (*8*), but in O_2-evolving PS II, the absorption peak is more intense after a 15 min illumination. This absorbance feature has been assigned to a Car neutral radical that is formed by deprotonation of a Car cation radical (*31*).

As observed previously, illumination of Mn-depleted PS II core complex preparations that were treated with hydroxylamine to reduce the tetranuclear manganese cluster results in the formation of Chl^+ species that are stable in the dark at 20 K. However, it is possible that hydroxylamine may also react with the protein or the Chls, altering the redox potentials of the cofactors or the structure of the protein. As an alternative to hydroxylamine treatment, we prepared Mn-depleted PS II by incubating with ascorbate for several hours (4−12 h) in the dark, which results in loss of O_2-evolving activity. In addition to reducing the Mn_4Ca cluster, ascorbate also reduces Cyt b_{559}, and the near-IR spectrum showed that only a small amount of Car^+ is formed in this sample by low temperature illumination because Cyt b_{559} is the lowest potential center and is preferentially photooxidized. But, after addition of ferricyanide to the Mn-depleted sample to reoxidize the heme, the light-minus-dark difference spectrum appears similar to the spectra previously observed for hydroxylamine-treated Mn-depleted PS II (Supporting Information Figure S2). We hypothesize that depletion of Mn_4Ca cluster may disrupt the structure of PS II and introduce structural heterogeneity in the PS II core complex because it is known from biochemical and structural studies that the ligands to the Mn_4Ca cluster are located in the D1 and CP43 polypeptides. The altered conformation may disrupt electron-transfer pathways by inducing small changes in the distances between cofactors. Depletion of Mn_4Ca may also affect the redox potentials of some of the Chl/Car in the protein, resulting in some Chl/Car becoming more or less favorable for oxidation.

Because broad near-IR absorption bands have been reported for di-μ-oxo-bridged Mn_2 inorganic model complexes in the 700−1000 nm region (*35*), we must address the possibility that these absorbance features result from the Mn_4Ca cluster. It is known that the OEC has a weak near-IR transition associated with the S_2 state, which can be converted from the EPR multiline signal ($S = 1/2$) to the $g \sim 4.1$ form by near-IR irradiation ($\lambda_{max} = 820$ nm) (*36*). The Mn_4Ca cluster has also been probed by resonance Raman spectroscopy using near-IR excitation wavelengths (*37*). However, the resonance Raman scattering is weak, which implies the extinction coefficient of the Mn_4-based transition is weak, similar to the electronic transitions of Mn_2 model complexes that are in the range of 60 M^{-1} cm^{-1} (*35*). This value is on the order of 100× smaller than the extinction coefficient of a Chl cation radical (7000 M^{-1} cm^{-1}), suggesting that at the concentration of PS II used in our measurements, it is not likely that Mn-cluster transitions contribute significantly to the near-IR spectra of either the nonilluminated or illuminated samples.

By several experiments, we demonstrate that the additional near-IR absorption species are Car^+, Chl^+, and $Car^\bullet$ and these species are intermediates of the secondary electron-transfer pathways. As shown previously by EPR, Y_D competes with Car and Chl as an electron donor to P_{680}^+, resulting in a lower yield of the Chl^+/Car^+ EPR signal at high pH (*7*). We also observe a lower yield of Car^+ and the Chl^+ signals by near-IR spectroscopy at higher pH (Supporting Information Figure S3). Because the sample is treated with ferricyanide, Cyt b_{559} is oxidized prior to freezing the sample and the heme cannot donate an electron to any of the cation radical species formed by photooxidation. We also find that if the sample is treated with ascorbate to reduce Cyt b_{559}, then none of the Chl and Car radical species form; instead, Q_A is reduced and Cyt b_{559} is oxidized (*38*). The observation that Y_D and Cyt b_{559} are competitive electron donors implies all of the redox-active Chl and Car species are intermediates of the secondary electron-transfer pathway.

We also examined formation of these species at warmer illumination temperatures from 85 to 160 K (Supporting Information Figure S4). The absorption peaks from charge separations that are less stable at 20 K are lower intensity at higher temperature. The Chl^+ peak maximum at 160 K is 810 nm, which appears to be the absorption maximum of the most stable Chl^+ species.

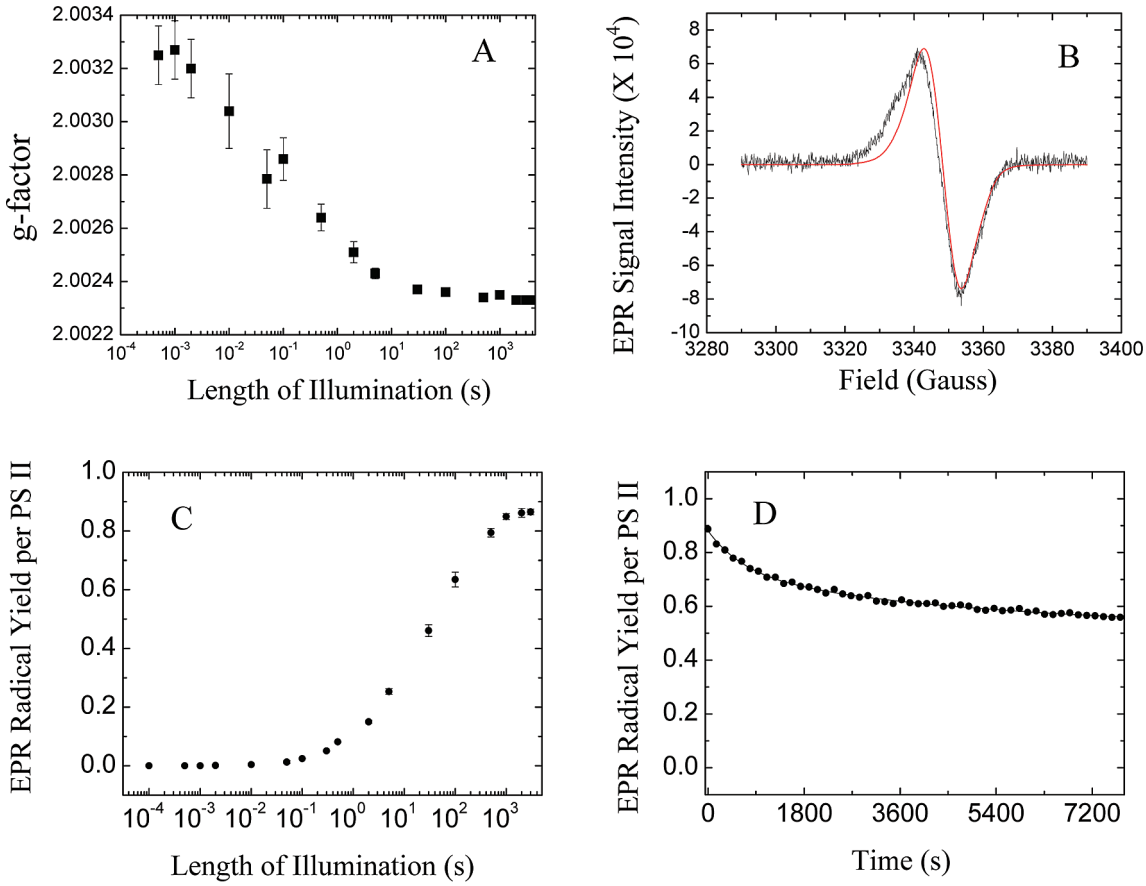

FIGURE 8: EPR measurements of O_2-evolving PS II core complexes. The *g*-value as a function of illumination time is shown in (A). Comparison of the EPR spectrum measured following a 50 ms flash of white light and the EPR spectrum recorded after 15 min illumination, normalized to the same peak-to-peak height (B). The EPR signal intensity is plotted as a function of illumination time in (C). The dark decay of the light-induced EPR signal is shown in (D). EPR conditions were: microwave frequency, 9.38 GHz; temperature, 30 K; modulation amplitude, 4 G; microwave power, 0.004 mW. Chl concentration was 2.0 mg/mL, pH = 6.0, with 5 mM ferricyanide.

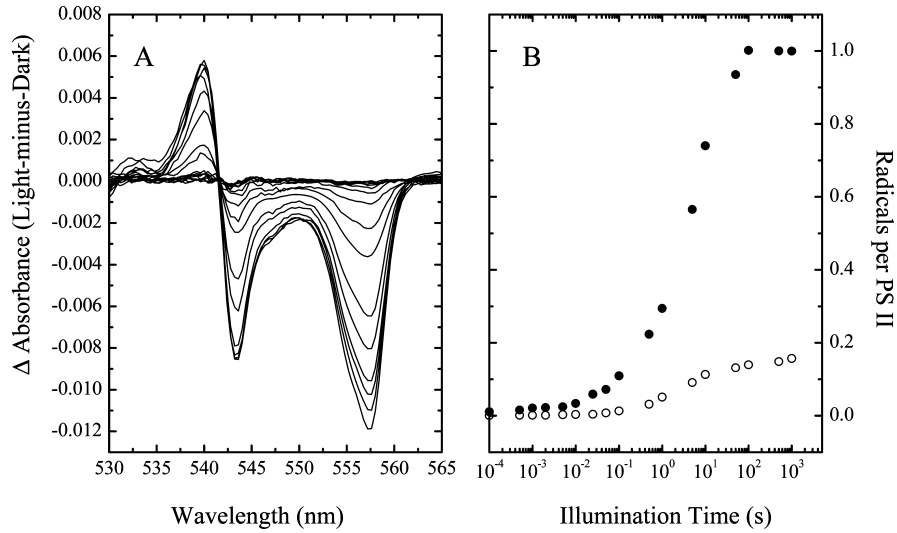

FIGURE 9: Light-minus-dark absorption spectra of O_2-evolving PS II showing the C550 electrochromic feature and Cyt b_{559} photooxidation at 20 K as a function of illumination time (A). Calculated yields of photoreduced Q_A (solid circles) and photooxidized Cyt b_{559} (open circles) per PS II (B). Chl concentration is 0.15 mg/mL.

Chl^+ Spectral Variation in O_2-Evolving Photosystem II. The chlorophylls in PS II have been described as spectrally congested, as their UV−visible absorbance spectra overlap extensively. We find that, although the near-IR absorption peaks of oxidized Chl and Car species do overlap considerably, they are resolvable kinetically, as shown in Figures 3 and 4. The maxima of the Chl^+ absorbance peaks in O_2-evolving PS II exhibit variations that are likely a result of perturbation of the near-IR absorption bands by the local electrostatic environment of the Chls in PS II. The X-ray crystal structures of two other photosynthetic proteins, the light-harvesting complex II (LHC II) (*39*) and photosystem I (PS I) (*40*), determined at 2.7 and 2.5 Å resolution, respectively, also revealed heterogeneous Chl-binding sites

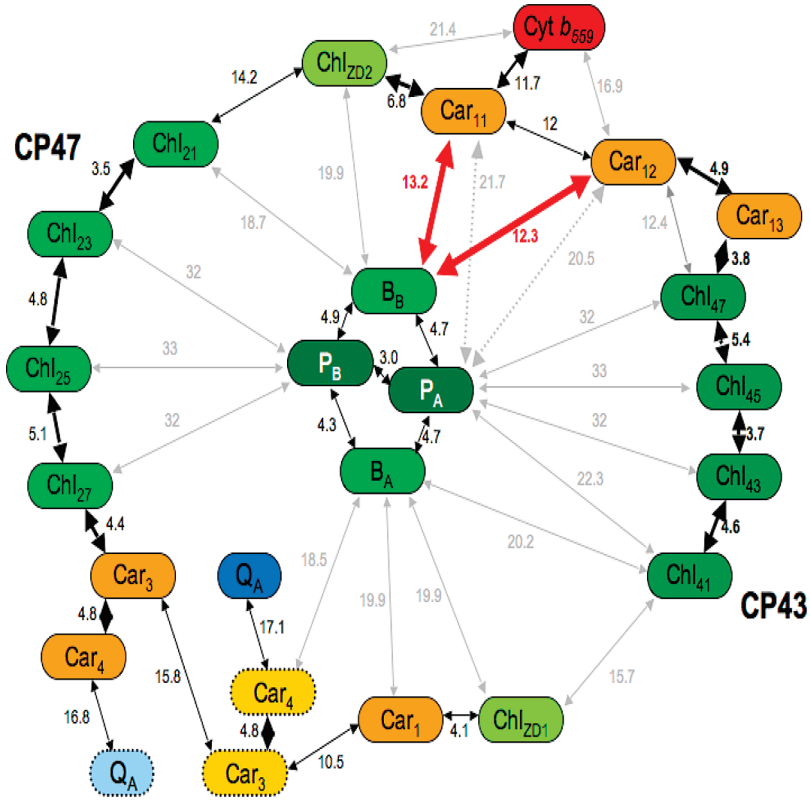

FIGURE 10: Schematic diagram of edge-to-edge distances between the core Chls, (P_A, P_B, B_A, B_B) and the nearby Chl and Car cofactors in the PS II core complex. The edge-to-edge distances are measured between the π-conjugated portion of the molecules in the Loll et al. X-ray crystal structure of PS II (*14*). Q_A surrounded by a dark-blue oval with solid line is (PQ9 53 in the Supporting Information) bound to the PS II reaction center. The Q_A bound to the other reaction center of the PS II dimer (PQ9 5053) is the light-blue oval surrounded by a dotted line. The shortest distance to Q_A is between Car_4 and the Q_A from the other PS II dimer (PQ9 5053) (PDB ID code 2AXT).

(*41*). We expect that the protein environment of PS II can tune the spectroscopic properties of Chl and Car. Variations within the PS II sample could also be present, either from freezing or functional heterogeneity due to different polypeptide composition (*42*).

It is possible that multiple near-IR absorption bands are due to the same species. In the molecular orbital model of chlorins and porphyrins, the electronic transitions from the HOMO to LUMO and the second highest occupied molecular orbital (SHOMO) to LUMO can occur and will depend on the symmetry of the transitions. The possibility of SHOMO transitions adds additional complication to interpreting these data because more than one of the peaks in the Chl^+ region may originate from the same species. Evidence in favor of this is that, if every spectral component is uniquely assigned in the quantization of Chl^+ in PS II, then the total Car^+ plus Chl^+ determined (from the near-IR spectrum) is slightly greater than 1.0 per PS II (Figure 6). However, the total radical yield measured by EPR is only 0.85 per PS II. Considering the uncertainty in the extinction coefficients for Chl and Car radicals, these values are in reasonable agreement. In addition, the different spectral components in the near-IR exhibit different kinetics of formation and decay, which argues that they arise from distinct species. However, it is possible that some of the Chl and/or Car radicals have two peaks in the near-IR.

Secondary Electron-Transfer Pathways. The structure of PS II fits with proposals that Car is the initial donor of the secondary electron-transfer pathway to P_{680}^+ (*14*). The edge-to-edge distance between P_A^+ and the Car or Chl will have the largest impact on the rate of electron transfer from Car to P_A^+. The rate also depends on the reduction potentials of the electron donors and acceptors, which will be affected by hydrogen bonding and the electrostatic environment of the protein. As a first approximation, we used the redox potentials calculated by Ishikita and Knapp (*29*) and the distances in the PS II structure to estimate the rates of Car and Chl oxidation by P_A^+ using the empirical equation for electron transfer over long distances developed by Dutton and co-workers (*43*). The two closest reaction center Car molecules (Car_{11} and Car_{12}) are 21.7 and 20.5 Å from P_A, the latter having an estimated rate of electron donation of 10^2 s^{-1} (see Figure 10). The carotenoid molecules Car_{11} and Car_{12} are also located in close proximity to B_B, (edge-to-edge distances of 13.2 and 12.3 Å), leading to a predicted rate of Car_{11} and Car_{12} oxidation via B_B of between 10^6-10^7 s^{-1}. However, oxidation of Car is known not to occur on such timescales (*2*). We conclude, therefore, that the main pathway of Car oxidation occurs via P_A, and both electron donors, Car_{11} and Car_{12}, compete.

The type of Chl^+ that forms depends on which Car is initially oxidized (see Figure 1). Car_{11} is located in the D2 protein near Chl_{ZD2}; thus, oxidation of this accessory Chl may occur rapidly. However, Car_{12} is slightly closer to P_A; if this Car is oxidized, it may rapidly oxidize Car_{13}, which is only 4.9 Å away (Figure 10). Car_{13} is located close to several carotenoid and chlorophyll molecules in CP43 (Figure 11). Therefore, it is likely that a cation radical on Car_{12} can easily migrate to the Chls in CP43.

Given the close proximity of the Chls within the inner antennae proteins CP43 and CP47 (4−6 Å), a cation radical in the antenna could rapidly move to other Chl and Car

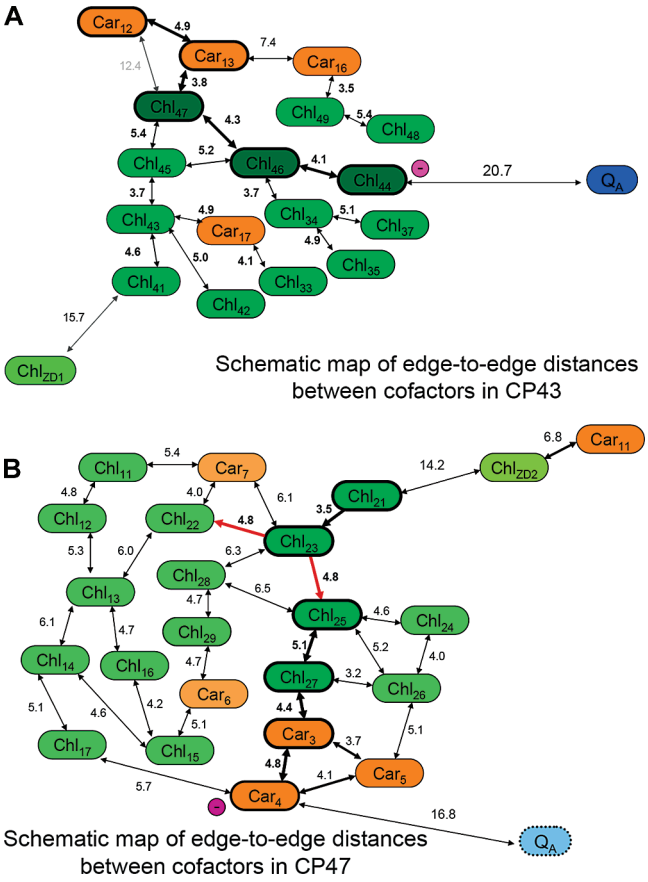

FIGURE 11: Schematic diagram of the edge-to-edge distances between Chl in CP43 (A) and CP47 (B). Distances were measured between the closest π-conjugated portion of the molecules in the Loll et al. X-ray crystal structure of PS II (*14*) (PDB ID code 2AXT).

because the rates of electron transfer among these densely packed pigment molecules are expected to be very fast (10^7-10^9 s^{-1}). Therefore, the cation radical will rapidly equilibrate among the Chl and Car and the thermodynamic distribution of the cation radical will depend on the relative Chl and Car redox potentials. At thermodynamic equilibrium, the hole will be located on the lowest potential electron donor within a given PS II complex. However, at low temperature (or high temperature), this equilibrium might not be achieved because a low-potential Chl/Car might be insulated by surrounding high-potential Chls. The pathway for forming a particular Chl$^+$ is not necessarily the same pathway for decay because the rate of each step depends on the ΔG of the electron donor and acceptor. The formation of a Chl$^+$ by the forward reaction is allowed, but the reverse reaction may require thermal energy. Therefore, after the hole moves to the lowest potential donor, it may become trapped. Because recombination does not occur rapidly at low temperatures, this suggests that the hole becomes trapped on a Chl or Car that is far from Q_A^-. A pathway for oxidation of Chl$_{ZD1}$ via the Chl in CP43 exists, as suggested by Vasil'ev et al. (*16*), but the multiple Chl$^+$ observed in this work may also be located within CP43 or CP47 (Figures 10 and 11).

We note that there are two negatively charged lipids, phosphatidyldiacylglycerol (PG) and sulfoquinovosyldiacylglycerol (SQDG), identified in the X-ray crystal structure nearby Chl$_{44}$ in CP43. The phosphate-group oxygen of PG (molecule LHG 203) and the sulfate group oxygen of SQDG (SQD 204) are 6.8 and 10.6 Å, respectively, from the ring carbonyl of Chl$_{44}$. Although Chl$_{44}$ is the closest antennae chlorophyll to Q_A at 20.7 Å, which is similar to the distance between Q_A and Chl$_{ZD1}$ or Chl$_{ZD2}$, this is still a long distance for electron transfer. The charge of the lipids may decrease the reduction potential of Chl$_{44}^+$, resulting in localization of the cation radical to this Chl and giving a charge separation that is fairly stable to recombination with Q_A^-. The most stable Chl$^+$ absorbs at 810 nm, and this species may be Chl$_{44}$.

On the basis of the close proximity of Chl$_{ZD2}$ to Car$_{11}$ (6.8 Å), which is hypothesized to be one of the initially oxidized carotenoids, it is reasonable to assume that Chl$_{ZD2}$ is one of the Chl$^+$ formed rapidly in PS II. The decay of this Chl$^+$ species may proceed either by recombination with Q_A^- (however, the distance is >40 Å and, therefore, direct electron transfer between Q_A^- and Chl$_{ZD2}^+$ is unlikely), or it may be oxidized by Chl$_{21}$ in CP47 (14.2 Å). As described above for CP43, a Chl cation radical in CP47 could also rapidly move among the closely packed Chls and become trapped on a low-potential Chl or Car (Figure 11B).

Several short steps connect the Chl in CP47 to Car$_4$, the closest Car or Chl molecule in PS II to Q_A with an edge-to-edge distance of 16.8 Å. At the temperatures studied here, charge recombination likely occurs through Car$_4$. This implies a slow process of hole transfer from Chl$^+$ to Car$^+$, consistent with our previous observation that the Car$^+$ decay is multiexponential (*8*). If the hole is preferentially localized on Chl, then electron transfer from Car to Chl$^+$ would be energetically uphill. There are many examples of electron transfer in redox proteins occurring via high-potential intermediates if the overall process is thermodynamically favorable (*43*). Car$_4$ is an interface carotenoid that is close to the Chls of CP47 via electron transfer through Car$_3$. Interestingly, there are two molecules of SQDG located nearby the cluster of five Car molecules at the PS II dimer interface. By the same argument presented above for Chl$_{44}$ in CP43, the charged sulfate groups may decrease the redox potentials of these carotenoids, making them more energetically accessible to participate in the secondary electron-transfer reactions.

Some evidence for hole migration to the lowest potential Chl is observable in the near-IR measurements at low temperature (Figure 4G). An increase in absorbance is observed at 840 nm as the species absorbing at 814, 793, and 750 nm decay. The rise can be fit by two half-lives of 200 and 700 s^{-1}. The rise of the 840 nm absorption feature occurs in the dark and suggests that the cation radical is migrating among the Chls in the PS II core complex. If we assume that this overall process is exergonic and has a possible range of ΔG that corresponds to the range of potentials calculated for Chls in the complex (using the values calculated for Chl in PS II between +742 and +1113 mV, or $\Delta G = -0.371$ to 0 eV (*29*)), we calculate a distance for this electron-transfer process to be between 25.8 and 28.6 Å for the 200 s^{-1} component and between 26.7 and 29.5 Å for the 700 s^{-1} component (*43*). Several possible Chl−Chl pairs are within this range of distances.

In previous work, the chlorophyll cation radical observed at 820 nm in Mn-depleted PS II from *Synechocystis* PCC 6803 was assigned to Chl$_{ZD1}$, based on site-directed mutagenesis and resonance Raman spectroscopy (*9*). However, in Mn-depleted spinach PS II membrane samples, it is

interesting to note that two near-IR Chl^+ absorption peaks are observed, one at 820 nm and a larger peak at 850 nm; the two peaks were attributed to chlorophyll cation radicals on Chl_{ZD1} and Chl_{ZD2} (*8*). The location of the 850 nm species is unknown, but, based on this analysis of the PS II X-ray crystal structure, it may be located in the antennae proteins CP43 and/or CP47.

CONCLUSIONS

We have characterized the formation and decay of near-IR absorption bands in light-minus-dark difference spectra of oxygen-evolving PS II core complexes illuminated at cryogenic temperatures. By using these kinetics data, together with Gaussian deconvolutions of the near-IR spectra, we resolve five absorption peaks that are attributed to chlorophyll cation radicals: two fast-decaying species at 793 and 814 nm and three slow-decaying species at 810, 825, and 840 nm. On the basis of the relatively slow rates of charge recombination of these chlorophyll cation radicals with Q_A^-, we conclude that the chlorophyll cation radicals observed here must be located on chlorophylls that are peripheral to the core chlorophylls of the PS II reaction center. Two of these are likely to be Chl_{ZD1} and Chl_{ZD2}, as previously proposed. However, the number of distinct Chl^+ species is larger than two, which requires that the secondary electron-transfer pathways include pigment molecules in the light-harvesting proteins CP43 and CP47 of PS II. This is the first evidence that Chls in the light-harvesting proteins CP43 and CP47 are oxidized by P_{680}^+. Although the yield of these Chl^+ species at room temperature is low, they may have a role in photoprotection of PS II, either by functioning in dissipative cyclic electron-transfer reactions or by quenching Chl fluorescence.

ACKNOWLEDGMENT

We thank Russ Bernardo for the construction of clamps for the cryostat in the near-IR spectrometer and the Teflon plunger for the cuvettes, Natasha Keith for reconstructing and greatly enhancing the nitrogen-purge plexiglas box for transferring samples into the cryostat, James McEvoy for careful reading and comments on the manuscript, and Phil Romero for assistance in measuring the edge-to-edge distances of cofactors in the crystal structure of PS II.

SUPPORTING INFORMATION AVAILABLE

The temperature dependence of the formation of Chl^+ and Car^+ measured by near IR spectroscopy and the pH dependence (at 20 K) of the formation of Chl^+ and Car^+ are described. The EPR spectra of the near-IR radical species formed as a function of illumination time are also described. This material is available free of charge via the Internet at http://pubs.acs.org.

REFERENCES

1. Dekker, J. P., and Van Grondelle, R. (2000) Primary charge separation in photosystem II. *Photosynth. Res. 63*, 195–208.
2. Diner, B. A., Schlodder, E., Nixon, P. J., Coleman, W. J., Rappaport, F., Lavergne, J., Vermaas, W. F. J., and Chisholm, D. A. (2001) Site-directed mutations at D1-His198 and D2-His 97 of photosystem II in *Synechocystis* PCC 6803: Sites of primary charge separation and cation and triplet stabilization. *Biochemistry 40*, 9265–9281.
3. McEvoy, J. P., and Brudvig, G. W. (2006) Water-splitting chemistry of photosystem II. *Chem. Rev. 106*, 4455–4483.
4. Faller, P., Fufezan, C., and Rutherford, A. W. (2005) Side-path electron donors: cytochrome b_{559}, chlorophyll Z and β-carotene, in *Photosystem II: The Light-Driven Water: Plastoquinone Oxidoreductase* (Wydrzynski, T. J., and Satoh, K., Eds.), pp 347−365, Springer Publishers, Dordrecht, The Netherlands.
5. Stewart, D. H., and Brudvig, G. W. (1998) Cytochrome b_{559} of photosystem II. *Biochim. Biophys. Acta 1367*, 63–87.
6. Feyziyev, Y., van Rotterdam, B. J., Bernat, G., and Styring, S. (2003) Electron transfer from cytochrome b_{559} and tyrosine(D) to the S_2 and S_3 states of the water oxidizing complex in photosystem II. *Chem. Phys. 294*, 415–431.
7. Faller, P., Rutherford, A. W., and Debus, R. J. (2002) Tyrosine D oxidation at cryogenic temperature in photosystem II. *Biochemistry 41*, 12914–12920.
8. Tracewell, C. A., Cua, A., Stewart, D. H., Bocian, D. F., and Brudvig, G. W. (2001) Characterization of carotenoid and chlorophyll photooxidation in photosystem II. *Biochemistry 40*, 193–203.
9. Stewart, D. H., Cua, A., Chisholm, D. A., Diner, B. A., Bocian, D. F., and Brudvig, G. W. (1998) Identification of H118 of the D1 polypeptide as the axial ligand to chlorophyll Z. *Biochemistry 37*, 10040–10046.
10. Telfer, A., Frolov, D., Barber, J., Robert, B., and Pascal, A. (2003) Oxidation of the two β-carotene molecules in the photosystem II reaction center. *Biochemistry 42*, 1008–1015.
11. Tracewell, C. A., and Brudvig, G. W. (2003) Two redox-active β-carotene molecules in photosystem II. *Biochemistry 42*, 9127–9136.
12. Hanley, J., Deligiannakis, Y., Pascal, A., Faller, P., and Rutherford, A. W. (1999) Carotenoid oxidation in photosystem II. *Biochemistry 38*, 8189–8195.
13. Faller, P., Pascal, A., and Rutherford, A. W. (2001) Beta-carotene redox reactions in photosystem II: Electron transfer pathway. *Biochemistry 40*, 6431–6440.
14. Loll, B., Kern, J., Saenger, W., Zouni, A., and Biesiadka, J. (2005) Towards complete cofactor arrangement in the 3.0 Å resolution structure of photosystem II. *Nature 438*, 1040–1044.
15. Kitajima, Y., and Noguchi, T. (2006) Photooxidation pathway of chlorophyll Z in photosystem II as studied by Fourier transform infrared spectroscopy. *Biochemistry 45*, 1938–1945.
16. Vasil'ev, S., Brudvig, G. W., and Bruce, D. (2003) The X-ray structure of photosystem II reveals a novel electron transport pathway between P_{680}, cytochrome b_{559} and the energy quenching cation, Chl_Z^+. *FEBS Lett. 543*, 159–163.
17. Vasil'ev, S., and Bruce, D. (2000) Picosecond time-resolved fluorescence studies on excitation energy transfer in a histidine 117 mutant of the D2 protein of photosystem II in *Synechocystis* 6803. *Biochemistry 39*, 14211–14218.
18. Koulougliotis, D., Innes, J., and Brudvig, G. (1994) Location of chlorophyll Z in photosystem II. *Biochemistry 33*, 11814–11822.
19. Kawamori, A., Katsuta, N., and Hara, H. (2003) Structural analysis of the three-spin systems of photosystem II by PELDOR. *Appl. Magn. Reson. 23*, 557–569.
20. Shigemori, K., Hara, H., Kawamori, A., and Akabori, K. (1998) Determination of distances from tyrosine D to Q_A and chlorophyll Z in photosystem II studied by "2 + 1" pulsed EPR. *Biochim. Biophys. Acta 1363*, 187–198.
21. Lakshmi, K. V., Poluektov, O. G., Reifler, M. J., Wagner, A. M., Thurnauer, M. C., and Brudvig, G. W. (2003) Pulsed high-frequency EPR study on the location of carotenoid and chlorophyll cation radicals in photosystem II. *J. Am. Chem. Soc. 125*, 5005–5014.
22. Faller, P., Rutherford, A. W., and Un, S. (2000) High-field EPR study of carotenoid($^{\cdot+}$) and the angular orientation of chlorophyll z($^{\cdot+}$) in photosystem II. *J. Phys. Chem. B 104*, 10960–10963.
23. Ishikita, H., Loll, B., Biesiadka, J., Kern, J., Irrgang, K. D., Zouni, A., Saenger, W., and Knapp, E. W. (2007) Function of two beta-carotenes near the D1 and D2 proteins in photosystem II dimers. *Biochim. Biophys. Acta 1767*, 79–87.
24. Lakshmi, K. V., Reifler, M. J., Chisholm, D. A., Wang, J. Y., Diner, B. A., and Brudvig, G. W. (2002) Correlation of the cytochrome c_{550} content of cyanobacterial photosystem II with the EPR properties of the oxygen-evolving complex. *Photosynth. Res. 72*, 175–189.
25. Erixon, K., and Butler, W. L. (1971) The relationship between Q, C-550 and cytochrome b_{559} in photoreactions at −196 degrees in chloroplasts. *Biochim. Biophys. Acta 234*, 381–389.

26. Buser, C. A., Diner, B. A., and Brudvig, G. W. (1992) Photooxidation of cytochrome b_{559} in oxygen-evolving photosystem II. *Biochemistry 31*, 11449–11459.
27. Buser, C. A., Diner, B. A., and Brudvig, G. W. (1992) Reevaluation of the stoichiometry of cytochrome b_{559} in photosystem II and thylakoid membranes. *Biochemistry 31*, 11441–11448.
28. Kaminskaya, O., Kern, J., Shuvalov, V. A., and Renger, G. (2005) Extinction coefficients of cytochromes b_{559} and c_{550} of *Thermosynechococcus elongatus* and cytochrome b_{559}/PS II stoichiometry of higher plants. *Biochim. Biophys. Acta 1708*, 333–341.
29. Ishikita, H., and Knapp, E.-W. (2005) Redox potentials of chlorophylls and β-carotene in the antenna complexes of photosystem II. *J. Am. Chem. Soc. 127*, 1963–1968.
30. Tang, X. S., and Diner, B. A. (1994) Biochemical and spectroscopic characterization of a new oxygen-evolving photosystem II core complex from the cyanobacterium *Synechocystis* PCC 6803. *Biochemistry 33*, 4594–4603.
31. Gao, Y., Shinopoulos, K. E., Tracewell, C. A., Focsan, A. L., Brudvig, G. W., and Kispert, L. D. (2008) Formation of carotenoid neutral radicals in photosytem II, *J. Phys. Chem. B*, submitted.
32. Borg, D. C., Fajer, J., Felton, R. H., and Dolphin, D. (1970) The π-cation radical of chlorophyll a. *Proc. Natl. Acad. Sci. U.S.A. 67*, 813–820.
33. Tan, Q., Kuciauskas, D., Lin, S., Stone, S., Moore, A., Moore, T., and Gust, D. (1997) Dynamics of photoinduced electron transfer in a carotenoid-porphyrin-dinitronaphthalenedicarboximide. *J. Phys. Chem. B 101*, 5214–5223.
34. Faller, P., Debus, R. J., Brettel, K., Sugiura, M., Rutherford, A. W., and Boussac, A. (2001) Rapid formation of the stable tyrosyl radical in photosystem II. *Proc. Natl. Acad. Sci. U.S.A. 98*, 14368–14373.
35. Gamelin, D. R., Kirk, M. L., Stemmler, T. L., Pal, S., Armstrong, W. H., Penner-Hahn, J. E., and Solomon, E. I. (1994) Electronic structure and spectroscopy of manganese catalase and di-mu-oxo [Mn(III)Mn(IV)] model complexes. *J. Am. Chem. Soc. 116*, 2392–2399.
36. Boussac, A., Un, S., Horner, O., and Rutherford, A. W. (1998) High-spin states ($S \geq 5/2$) of the photosystem II manganese complex. *Biochemistry 37*, 4001–4007.
37. Cua, A., Stewart, D. H., Reifler, M. J., Brudvig, G. W., and Bocian, D. F. (2000) Low-frequency resonance Raman characterization of the oxygen-evolving complex of photosystem II. *J. Am. Chem. Soc. 122*, 2069–2077.
38. Tracewell, C. A., and Brudvig, G. W. Characterization of the secondary electron-transfer pathway intermediates of photosystem II containing low-potential cytochrome b_{559}, *Photosynth. Res.*, in press (doi: 10.1007/s11120-008-9360-8).
39. Standfuss, J., Terwisscha van Scheltinga, A. C., Lamborghini, M., and Kühlbrandt, W. (2005) Mechanisms of photoprotection and nonphotochemical quenching in pea light-harvesting complex at 2.5 Å resolution. *EMBO J. 24*, 919–928.
40. Jordan, P., Fromme, P., Witt, H. T., Klukas, O., Saenger, W., and Krauss, N. (2001) Three-dimensional structure of cyanobacterial photosystem I at 2.5 Å resolution. *Nature 411*, 909–917.
41. Balaban, T. S., Fromme, P., Holzwarth, A. R., Krauss, N., and Prokhorenko, V. I. (2002) Relevance of the diastereotopic ligation of magnesium atoms of chlorophylls in photosystem I. *Biochim. Biophys. Acta 1556*, 197–207.
42. Veerman, J., McConnell, M. D., Vasil'ev, S., Mamedov, F., Styring, S., and Bruce, D. (2007) Functional heterogeneity of photosystem II in domain specific regions of the thylakoid membrane of spinach (*Spinacia oleracea L.*). *Biochemistry 46*, 3443–3453.
43. Page, C. C., Moser, C. C., and Dutton, P. L. (2003) Mechanism for electron transfer within and between proteins. *Curr. Opin. Chem. Biol. 7*, 551–556.

BI801461D